Materials Transactions, Vol. 45, No. 5 (2004) pp. 1706 to 1713

Tear Toughness of Permanent Mold Cast and DC Cast A356 Aluminum Alloys

Shinji Kumai, Toshikazu Tanaka*1, Hong Zhu*2 and Akikazu Sato

Department of Materials Science and Engineering, Tokyo Institute of Technology, Yokohama 226-8502, Japan

Cast products of A356 with different microstructural features were prepared; permanent-mold cast (PM) and direct-chill cast (DC) products. For each casting, a sharp notched plate specimen was subjected to static tensile loading until a crack initiated at the notch root and propagated across the width of the specimen. Both maximum load and energy to fracture (the integrated area under the load-displacement curve) increased with decreasing dendrite arm spacing (DAS). The curve of DC was smooth and the energy to fracture was quite large. The load-displacement curve was divided into two segments by a vertical line through the maximum load. The area under the first segment is a measure of the energy necessary to initiate the crack. The second segment represents the energy necessary for crack propagation. Unit energy was computed by dividing the measured energy by the net area of the specimen. Refinement of DAS and grain size increased unit energies for crack initiation (UEi) and propagation (UEp). Comparison among PM products revealed that DAS refinement was effective for increasing UEi. Among the present castings, the DC product with the finest DAS exhibited a significant increase in UEp. Observation of the crack propagation path revealed that the fracture surface was normal to the loading direction for PM. In contrast, for DC, a slanted crack path was dominant through the specimen ligament. The features of the crack propagation path are considered to have affected quantitative balance between UEi and UEp. The increased UEp in DC is considered to be due to the introduced slanted crack. Tear tests were confirmed to provide useful information concerning the effect of solidification structure on toughness, which can serve as a guide for further toughening of aluminum alloy castings.

(Received September 30, 2003; Accepted March 4, 2004)

Keywords: *tear toughness, A356 alloy, permanent-mold cast, direct-chill cast, unit energy, solidification structure*

1. Introduction

The casting process provides great economic advantages in reducing overall costs for manufacturing complex three-dimensional structures. Production of cast and die-cast aluminum alloys in Japan has increased steadily, amounting to around 381000 tons and 750000 tons in 2001, respectively. These products are mainly for automotive use, which accounts for 91% of total production of cast aluminum and 78% of total production of die-cast alloys. Cast and die-cast aluminum alloys have traditionally been used as lightweight structural materials for automotive engines, such as engine blocks and cylinders.

Global environmental problems which have emerged in recent years require further weight reduction of automobiles in order to conserve energy and reduce exhaust gas emission. This promotes the non-traditional use of lightweight aluminum alloy cast products in automobiles. For example, application to load-carrying machine parts is being pursued as a viable alternative to wrought or forged aluminum alloy products, and requires high toughness.

Under normal conditions, castings are known to exhibit mechanical properties inferior to those of wrought products. In particular, tensile ductility and fracture toughness of the castings tend to exhibit great variance throughout a given component. This results from the inevitable inclusion of some kinds of casting defects during the solidification process. Inhomogeneous solidification structure is another possible reason for the unstable mechanical properties. Therefore, in order to develop high-quality cast products which can be used in the load-carrying applications, we must elucidate the relationships among toughness, casting defects and solidified structure.

Toughness of metallic materials is evaluated quantitatively by either K_{IC} or J_{IC}. Obtaining K_{IC} values is difficult for most aluminum alloys, since they have moderate strength and high ductility. Specimen size required for obtaining valid K_{IC} values may reach the order of magnitude of a meter. From the viewpoint of restriction on specimen size, J_{IC} tests are better than K_{IC} tests for aluminum alloys. However, the J_{IC} test procedure is complicated, as is the K_{IC} procedure.

Therefore, another type of toughness test is strongly desired by foundry engineers and researchers who are involved in the development of high-performance aluminum alloy castings. The toughness test method should be not only reliable, but also simple and convenient.

Toughness of aluminum alloys can be estimated from tear resistance obtained by a tear test standardized in ASTM B871.[1] In the tear test, sharp-notched plate specimens are subjected to static tensile loading until a crack initiates at the notch root and propagates across the width of the specimen. The energy for crack initiation and the energy for propagation are obtained from the recorded load-displacement curve. Unit crack propagation energy is the representative criterion of tear toughness. Continued use of the tear test[2,3] has provided extensive background data. Correlation of these data with the results of other tests of fracture characteristics indicates that the tear test is more than just a relative rating, and in fact is a quantitative measure of crack toughness. To date, unit energies for tear fracture have been used to rate the toughness of various kinds of aluminum alloy products.[2–6] However, researches on cast aluminum alloy products have been very limited.[2,7]

The purpose of the present study is to examine availability and practicability of the tear test as a guide for evaluating fracture toughness of castings and die-castings.

*1Graduate Student, Tokyo Institute of Technology. Present address: Sumitomo Light Metal Industries, Ltd., Nagoya 455-8670, Japan

*2Graduate Student, Tokyo Institute of Technology

2. Experimental Procedure

2.1 Materials

The material selected in the present study is A356 aluminum alloy, which belongs to the most widely used aluminum-silicon alloy system. The hypo-eutectic Al-7%Si-(0.3∼0.4)%Mg alloy is commonly specified as a cast aluminum alloy for automotive applications. The alloy, having a low Fe content, is known as a premium alloy and corresponds to JIS AC4CH in Japan. Microstructural features of the alloy are characterized by grain size, primary aluminum secondary dendrite arm spacing (DAS), and morphology and distribution of eutectic Si particles and inclusions and casting defects. The matrix also includes precipitation structure, since the alloy is capable of being age-hardened. For permanent mold castings, various mold temperatures were chosen in order to control the microstructural factors systematically.

The present study employed both permanent-mold cast and direct-chill cast products. These were supplied by the research committee of light metallic alloys at the Japan Foundry Engineering Society. The fabrication procedure employed for permanent mold castings (called PM hereafter) was as follows. A356 alloy ingots were melted at 973 K and degassed by injecting bubbles of argon gas through a rotating nozzle in order to reduce hydrogen content. After the first degassing, an Al-10 mass%Sr alloy was added to the melt for the purpose of eutectic Si modification. The second degassing was performed, and then the molten metal was poured into a permanent mold made of cast iron. The present permanent mold is standardized in JIS H5202,[8] which is designed for producing a sound aluminum alloy casting. Three different mold temperatures (723, 573 and 423 K) were employed in order to obtain castings which solidified at different cooling rates. These resultant castings are called PM1, PM2 and PM3 respectively. The size of each casting was about $30 \times 40 \times 200$ (mm). Throughout the fabrication process, special attention was paid to minimize both the incorporation of casting defects and the spread of microstructure between batches.

The direct-chill cast product (called DC hereafter) was a continuous rod measuring 84 mm in diameter. DC casting is a semi-continuous casting process. Water-cooled molds initiate the first stage of solidification, and water sprays impinge on the shell of solid aluminum enclosing the still-liquid core. As compared with the ordinary permanent-mold castings, DC castings generally have finer solidification structure and fewer casting defects. DC cast material is normally used for producing rolling ingots (slabs) and extrusion ingots (billets).

Table 1 shows the chemical compositions of these materials. Although the materials exhibit slight differences in silicon and magnesium content, their chemical composition is essentially identical.

Table 1 Chemical compositions of permanent-mold cast (PM) and direct-chill cast (DC) materials.

(mass%)

	Si	Mg	Fe	Ti	Cu	Mn	Sr	Al
PM	7.1	0.39	0.12	0.11	0.03	0.01	0.008	bal
DC	6.8	0.29	0.12	0.12	0.03	0.01	0	bal

2.2 Heat treatment

The cast materials were homogenized at 808 K for 28.8 ks (8 h) and water-quenched. After being maintained at room temperature for 43.3 ks (12 h), they were aged at 433 K for 21.6 ks (6 h). This corresponds to T6 treatment.

2.3 Microstructural observation

Following heat treatment, the polished cross-section of the casting was optically examined for observation of microstructure. An image analyzer was employed for quantitative evaluation of secondary dendrite arm spacing (DAS), and size and aspect ratio of eutectic Si particles. A polished cross-section was also anodized in a 2% HF solution at a voltage of 25 V and a current density of 0.2 mAmm^{-2}. The anodized sample exhibited a clear grain structure image under polarized light in an optical microscope.

2.4 Tensile tests

Small-size round-bar specimens (gage section: ϕ6.25 mm $\times$ 32 mm) were machined from the PM cast and DC cast products and provided for the test. This scheme was employed to obtain as many specimens as possible from a single cast product. Monotonic tensile tests were performed using an Instron-type testing machine at a constant crosshead speed of 8.3×10^{-6} ms^{-1} at room temperature in air.

2.5 Tear tests

Testing procedure of the tear test is standardized in ASTM B871.[1] Figure 1 shows the specimen used in the present study. This is almost equivalent to the designated specimen size in the standard, except that the thickness (7 mm) is slightly greater than specified in the standard.

Tear tests were performed using an Instron-type testing machine. The device for transmitting load to the specimen was such that the load axis coincided with the root of the edge notch. As shown in Fig. 2, the arrangement of load application incorporated clevises having hardened pins which pass through the holes in the specimen. The specimen was subjected to tensile loading at a constant crosshead speed of 8.3×10^{-6} ms^{-1} at room temperature in air.

Change in load and crosshead displacement was recorded in order to obtain the load-displacement curve. It should be mentioned that the standard recommends the use of displacement gages which are mounted on the specimen or the clevis. If crosshead displacement is used in the displacement

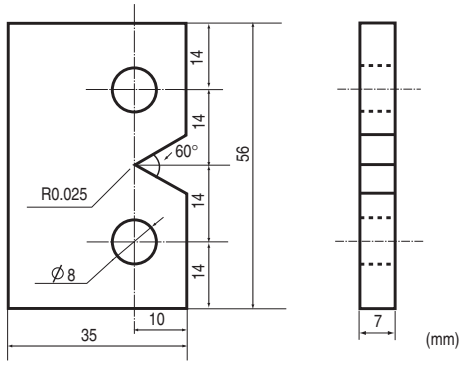

Fig. 1 Tear test specimen.

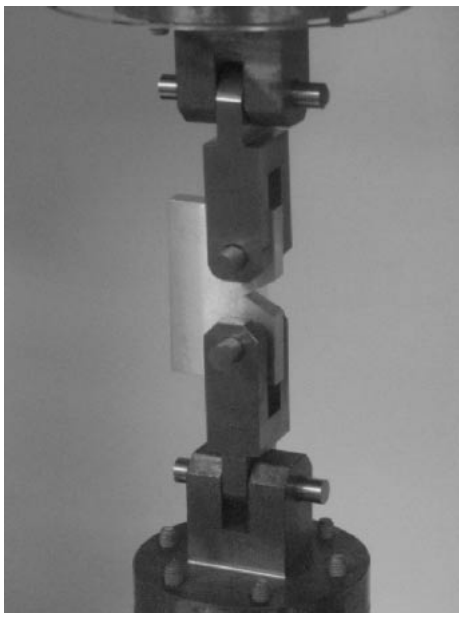

Fig. 2 Specimen and clevises for loading in the tear test.

measurement, deformation in the test fixtures and specimen clevis is included in the displacement measurement and it contributes to the apparent initiation and propagation energies measured possibly. Consequently, the data obtained cannot be compared directly with data measured by using other testing system. In the present study, however, we dared to adopt crosshead displacement. The motivation for this decision was that foundry engineers and researchers require a simple, convenient toughness test method. In addition, the present authors performed a number of tear tests for some cast alloys comparable to the present material using the displacement gage in advance. Experience based on a series of experiments has shown that load-displacement curves obtained in the present study are still useful for direct comparison and relative rating of tear toughness of the A356 cast products so long as we use exactly the same testing machine and loading system.

3. Experimental Results and Discussion

3.1 Solidification structure and tensile properties of the cast products

Figures 3(a)–(d) show optical micrographs of the T6 treated PM and DC castings. Both castings exhibit an ordinary dendrite structure of the hypo-eutectic Al-Si base

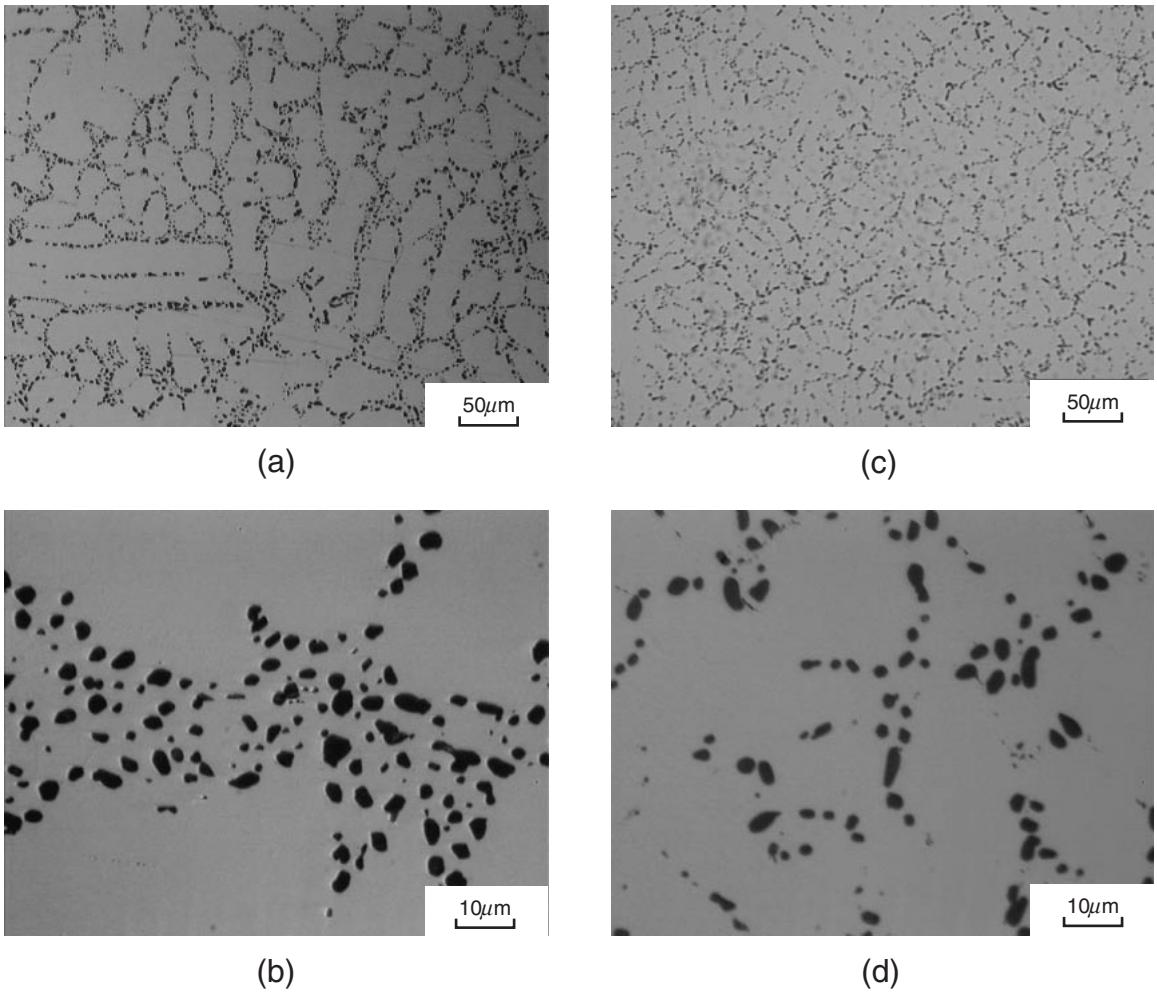

Fig. 3 Optical micrographs of the T6 treated PM and DC castings. (a) dendrite structure of PM, (b) eutectic Si particles of PM, (c) dendrite structure of DC, (d) eutectic Si particles of DC.

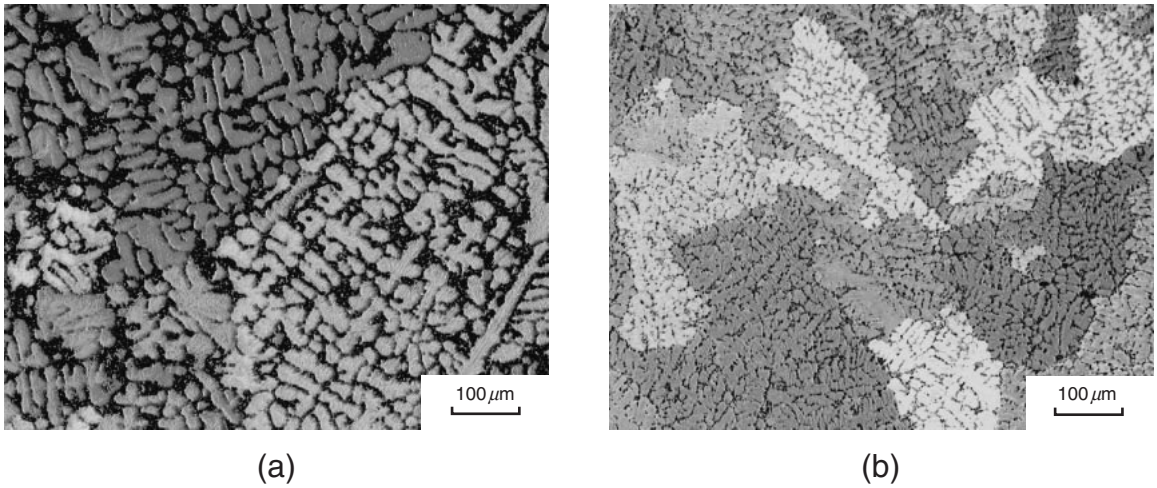

Fig. 4 Optical micrographs of anodized structure of the T6 treated PM and DC castings. (a) grain structure of PM, (b) grain structure of DC.

Table 2 Quantitative data of microstructural factors of PM and DC cast products.

	GS (μm)	DAS (μm)	Si (μm)	Aspect ratio
PM1	769	44.4	2.9	1.6
PM2	508	27.4	2.6	1.5
PM3	612	26.7	2.6	1.6
DC	216	13.3	2.5	1.6

alloy. Eutectic Si particles are located at dendrite cell boundaries. Figures 4(a) and (b) show optical micrographs of the anodized samples. The grain structure can be clearly seen from the difference in tone of color.

Table 2 shows quantitative data on microstructural parameters: grain size, DAS, and size and aspect ratio of eutectic Si particles. PM1, 2, and 3 correspond to the permanent mold cast products, whose mold temperatures were 723, 573, and 423 K, respectively. The effect of mold temperature is evident when we compare PM1 and PM3 in terms of DAS. Higher mold temperature resulted in slower cooling rates and consequently larger DAS. DC exhibits the smallest DAS as well as the smallest grain size. The present materials exhibit no significant difference in the size and morphology of Si particles. The relatively long homogenization time adopted in the present study is considered the likely reason for well-coarsened globular Si particles in all cast products.

Tensile properties of the cast products are summarized in Table 3. Both strength and ductility are low in PM1, which among the specimens exhibit the largest grain size, DAS and Si particle size. The DC specimen with fine grain size and DAS exhibits the greatest elongation. Relatively low proof stress in DC may be due to lower Mg content than PM, resulting in a lower volume fraction of precipitates for age-hardening.

Table 3 Tensile properties of PM and DC cast products.

	$\sigma_{0.2}$ (MPa)	UTS (MPa)	Elongation (%)
PM1	220	275	7
PM2	230	305	13
PM3	225	303	15
DC	220	298	23

Refinement of dendrite structure is also known to be effective for strengthening the hypo-eutectic cast Al-Si alloy. In particular, a Hall-Petch type relationship has been obtained between proof stress and $d^{-1/2}$ (d: DAS).[9] The present results, however, disagree with this general result. In spite of a significant difference in DAS between PM and DC products in Table 2, their proof stress values are almost same, as shown in Table 3.

The following is one of the possible reasons. In the present study, both microstructural observation and tensile tests were performed after the T6 treatment. In all the present castings, the 8-hour homogenization included in the present T6 treatment was sufficient to change eutectic Si particles to a similar globular morphology. Therefore, in the present case, refined Si particles, which are generally accompanied by refined DAS, may exhibit diminished effect on strength. A reduced contribution of age-hardening for DC products is also anticipated, since, as shown in Table 1, Mg content of DC is lower than that of PM. This may result in a moderate increase in proof stress of DC product despite its refined DAS structure.

3.2 Effects of solidification structure on tear toughness of the cast products

Figures 5(a)–(c) show load-displacement curves for PM1, 2, and 3. Pop-in, such as instantaneous load drop, was observed before the load reached the maximum. Both the maximum load and the area under the load-displacement curve increased with decreasing DAS. The load-displacement curve for DC in Fig. 5(d), differs from those of the PM group. The curve is smooth and gentle, and the area under the load-displacement curve is quite large. We should mention that in the present study crosshead movement of the test machine was set to stop when the load decreased to 1 kN.

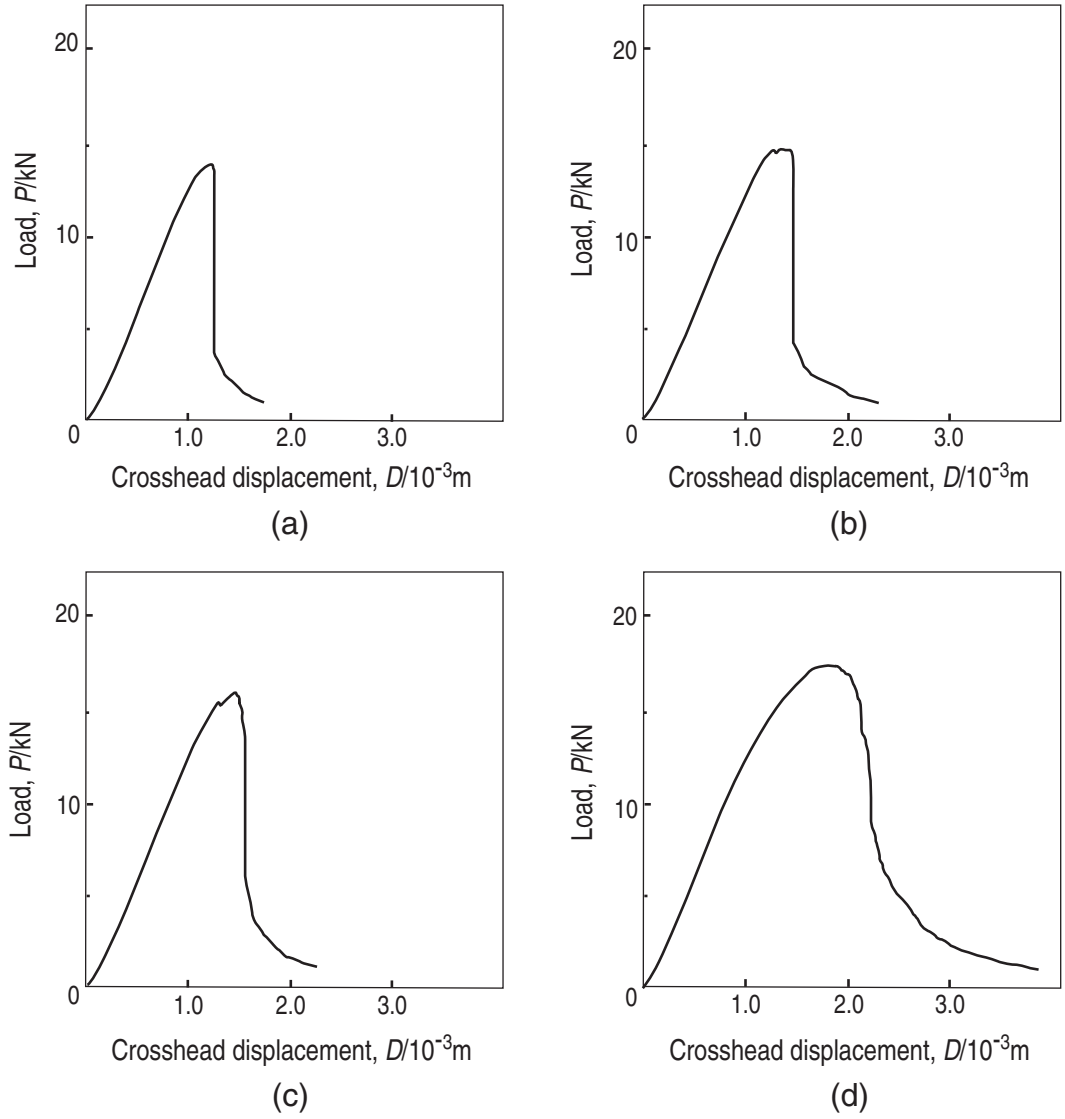

Fig. 5 Load-displacement curves for PM1, PM2, PM3, and DC cast products. (a) PM1, (b) PM2, (c) PM3, (d) DC.

Therefore, none of specimens completely fractured in half.

All load-displacement curves are shown together in Fig. 6 in order to facilitate comparison. Decrease in DAS was found to be effective for increasing both maximum load and energy to fracture. Fine grain size of DC (about 1/3 of those of the PM products) is also considered to result in the increased fracture energy.

Microstructural control of the casting is normally achieved by changing cooling rates. Controlling individual microstructural factors at will is difficult since they all differ in cooling rate dependency. The manner in which casting defects are formed is also dependent on cooling rate and is quite sensitive to the fabrication process. In the present study, only mold temperature was changed, because we wanted to produce a series of PM products with different DAS while keeping other microstructural factors as intact as possible. As mentioned previously, the T6 heat treatment including 8-hour homogenization was also helpful for highlighting the effect of DAS.

As illustrated schematically in Fig. 7, the vertical line through the maximum load divided the load-displacement

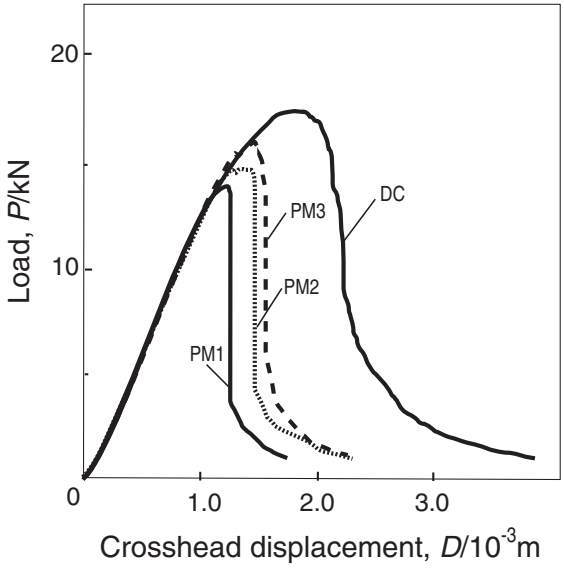

Fig. 6 Comparison among load-displacement curves of PM and DC cast products.

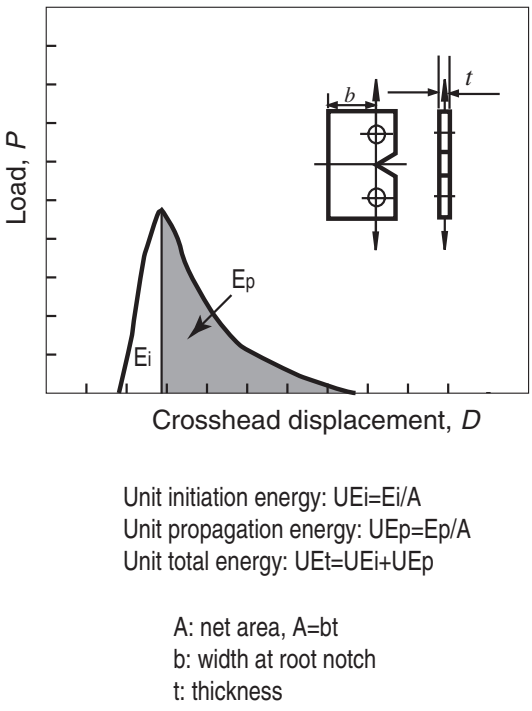

Fig. 7 A schematic load-displacement curve and definitions of crack initiation and crack propagation energies.

curve into two segments; crack initiation and crack propagation. The area under the first segment of the curve is a measure of the energy necessary to initiate the crack. The area under the second segment represents the energy necessary for the crack to propagate across the specimen. Each energestic value is obtained by integrating the area under the curve concerned. Load-displacement area measurement was carried out when load exceeded 1 kN.

ASTM B871[1)] designates three energestic parameters for evaluating tear toughness: Unit crack initiation energy (UEi), Unit crack propagation energy (UEp) and Unit total energy (UEt). Unit energy is computed by dividing the measured energy by the net area of the specimen. In the present tests, none of specimens fractured completely, because the test was stopped when the load dropped to 1 kN. However, the tested specimens were comparable in area of ligament remaining. Therefore, we adopted the original ligament area (25 mm × 7 mm) as net area. Table 4 shows the obtained UEi, UEp and UEt values of each cast product for comparison.

In ASTM B871, UEp is recognized as the primary result of the tear test. However, in some previous studies,[4–6)] UEi was also used to evaluate tear toughness because of conceptual similarity between UEi and K_{IC} (J_{IC}). In the present study, both UEi and UEp (consequently, UEt) are considered to be reasonable indicators for expressing the effect of solidification structure.

DAS refinement is found to be effective for increasing UEi in all cast products. Meanwhile, a significant increase in UEp value is found in the DC products; It is five times that in PM products. Such quantitative balance between UEi and UEp is considered to result from the features of crack propagation, as described in the following section.

Table 4 Unit energies obtained from load-displacement curves for PM and DC cast products.

	UEi (kNm^{-1})	UEp (kNm^{-1})	UEt (kNm^{-1})
PM1	38.3	9.3	47.5
PM2	43.7	10.5	54.2
PM3	53.4	10.6	64.0
DC	77.7	52.6	130.3

3.3 Effects of crack propagation path on tear toughness of the cast products

Figures 8(a) and (b) show macroscopic appearance of the tear tested specimens. Figures 9(a) and (b) schematically illustrate the observed crack propagation path for each cast product. For PM specimen (Fig. 9(a)), a flat crack was formed. The fracture surface was normal to the loading direction through the net section of the specimen. In contrast, in DC specimens a slanted crack path was dominant through the specimen ligament (Fig. 9(b)). The fracture surface was entirely covered with the slanted crack. Both disappearance of the small load drop in the load-displacement curve and the

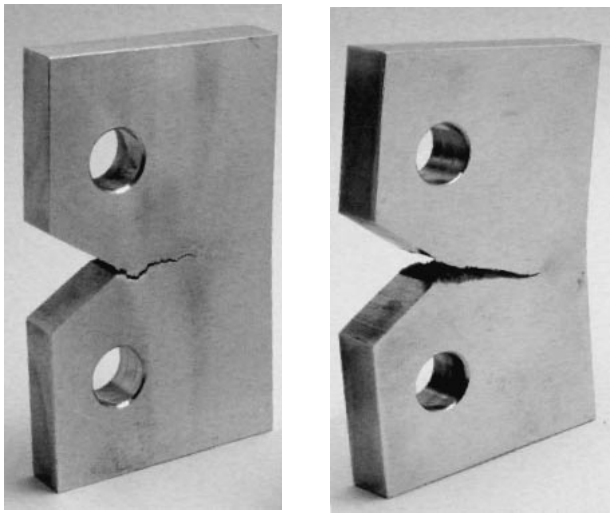

Fig. 8 Macroscopic appearance of the cracked tear test specimens. (a) PM, (b) DC.

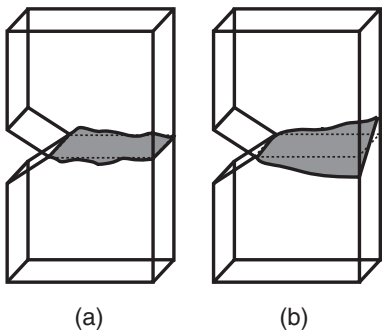

Fig. 9 Schematic illustrations of the crack propagation path for PM and DC cast products. (a) PM, (b) DC.

increased UEp in DC are considered to be due to the introduced slanted crack.

The relationship between increased fracture resistance and slanted crack path has been investigated from a fracture mechanistic approach. From a review of the literature of fracture mechanics, the effect of stress state on the macroscopic appearance of fracture path is explained as follows. When a pre-cracked specimen is monotonically loaded to fracture, crack extension starts macroscopically flat but is immediately accompanied by small shear lips at the side surfaces. A change in the planes of maximum shear stress plays an important role in this change. Under plane-strain conditions a "hinge" type deformation is followed by flat fracture. Meanwhile, under plane-stress conditions slant fracture occurs by shear from hinge-type initiation.[9,10] Ideally a critical stress intensity factor, K_c, associated with a specific crack geometry can be used to predict toughness of the material. However, K_c depends on test temperature, specimen thickness, and constraints. As is well known, plane-stress is dominant when the specimen is thin. Beyond a certain thickness the material is predominantly in plane-strain.

The effect of specimen thickness on fracture toughness for ductile materials was treated by Krafft *et al.* and Knott.[10–12] Krafft *et al.* supposed that the plastic deformation energy necessary for crack propagation is related to the area of the newly-created flat crack surface in plane strain. Meanwhile, in plane stress, the plastic energy is related to the volume contained by slanted crack surfaces. This is illustrated in Fig. 10. In the figure a specimen of thickness t is considered to crack with a fraction of s of the thickness in plane-stress and the remaining fraction $(1 - s)$ in plane-strain. For a crack growth increment da total energy consumption is

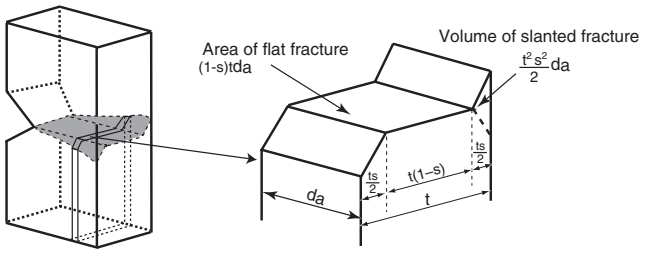

Fig. 10 Model of Krafft *et al.* for explaining the development of crack resistance.

$$dW = (dW_S/dA)t(1 - s)da + (dW_P/dV)(t^2s^2/2)da \quad (1)$$

where

dW_S/dA = energy consumption rate for plane-strain (per unit surface area),

dW_P/dV = energy consumption rate for plane-stress (per unit volume).

The crack resistance, R, is given by

$$R = (1/t)(dW/da) = (dW_S/dA)(1 - s) + (dW_P/dV)(ts^2/2) \quad (2)$$

As has been known, $dW_P/dV \gg dW_S/dA$. The model presented by Krafft *et al.* provides an explanation of the effect of specimen thickness on change in fracture mode.

Knott made the assumption that the absolute thickness of shear lips at the specimen side surfaces is approximately constant and the fraction of slanted crack (s in eq. (1)) decreases with increasing specimen thickness. He examined the relationship among fracture resistance, fraction of slant crack and the specimen thickness for 7075-T6 aluminum alloy sheet specimens. His experimental results agreed with the estimated results using eq. (2) very well. A fracture mechanistic approach indicated that the slant fracture increases fracture resistance or toughness, and its contribution depends on specimen thickness.

In contrast to the situation described above, in the present study specimen thickness was fixed to be 7 mm. In addition, proof stress was almost the same among the cast products. This suggests that all the notched (cracked) specimens are in the same stress conditions from the geometric point of view.

When the proof stress (yield stress) and specimen thickness are considered, all the present cast products were possibly in fully plane-stress or transitional plane-stress to plane-strain conditions. In this case, slant fracture was considered to be dominant in their fracture. However, this is true, only in DC products. PM products exhibited pseudo-flat fracture appearance.

A reasonable conjecture is that the differences in crack propagation path among the present cast products are attributed to microstructural differences. As shown in Table 2, DAS of DC is significantly smaller than that of PM products. Grain size is also refined in DC. The refined solidification structure of DC is considered to be beneficial for deformation as good as that of a wrought aluminum alloy product. This effect is also appeared in large tensile elongation as shown in Table 3. This is considered to result in slanted crack path, and consequently increases tear toughness. PM cast products have coarser microstructure than DC products. In addition, they were not completely free from inclusions and casting defects, although their quality was much better than that of conventional cast products. The incorporated inclusions and defects may act as preferential crack initiation sites or stress risers and facilitate the pseudo-flat fracture.

The present test results suggest that the tear tests can provide the useful information concerning the effect of solidification structure on toughness. The fracture toughness test based on the linear elastic fracture mechanics is not applicable to most aluminum alloys, because of limitations on specimen size. In contrast, the tear test is limited only by the capacity of the source of external loading.[3] The tear test is available to foundry engineers as a guide for further toughening of the aluminum alloy castings.

4. Conclusions

In order to examine the availability and practicability of the tear test as a guide for evaluating fracture toughness of castings, sharp notched plate specimens of A356 aluminum alloy castings with different microstructural features were each subjected to static tensile loading until a crack initiated at the notch root and propagated across the width of the specimen. Energy for crack initiation and propagation were obtained from the recorded load-displacement curve, and the effect of solidification structure on tear toughness was investigated. Refinement of dendrite arm spacing (DAS) and grain size increased unit energies for crack initiation (UEi) and propagation (UEp). Comparison among the permanent mold cast products (PM) with ordinary dendrite structure revealed that DAS refinement was effective for increasing UEi. Among the present castings, the direct-chill cast product (DC) with the finest DAS exhibited a significant increase in UEp. In PM specimens, fracture surface was normal to the loading direction. In contrast in DC specimens slanted crack path was dominant through the specimen ligament. Quantitative balance between UEi and UEp is considered to depend on the features of crack propagation. The increased UEp in DC is considered to be due to the introduced slant crack. The tear tests were confirmed to provide useful information concerning the effect of solidification structure on toughness, which is available as a reliable but simple and convenient tool for the development of aluminum alloy castings with improved toughness.

Acknowledgements

The authors would like to express their thanks to the research committee of light metallic alloys at the Japan Foundry Engineering Society for supplying cast materials and offering useful discussion. The authors also acknowledge the Light Metal Education Foundation, Inc. for providing partial financial support for this work.

REFERENCES

1) ASTM standard, Designation: B871-96, Standard Test Method for Tear Testing of Aluminum Alloy Products, (1996) 602–608.
2) J. G. Kaufmann and A. H. Knoll: Materials Research & Standards, April (1964) 151–155.
3) J. G. Kaufmann: Fracture Resistance of Aluminum alloys, The Aluminum Association, ASM International, ISBN: 0-87170-732-2 (2001) 38–74.
4) S. Komura and H. Taki: J. JILM **24**, 9 (1974) 399–405.
5) S. Komura and H. Taki: J. JILM **24**, 9 (1974) 406–410.
6) T. Kobayashi, M. Niinomi and K. Ikeda: J. JILM **38**, 1 (1988) 9–15.
7) S. W. Han, S. W. Kim and S. Kumai: Fatigue Fract. Engng Mater. Strct. **27**, 1, (2004) 9–17.
8) *JIS Handbook, Non-ferrous metals*, (Japanese Standard Association, 2001) 957–965.
9) T. Reinhart: Fatigue and Fracture Properties of Aluminum Alloy Castings, ASM Handbook, 19, ASM (1996).
10) J. F. Knott: *Fundamentals of Fracture Mechanics*, (Butterworths, London, 1973).
11) H. L. Ewalds and R. J. H. Wanhill: *fracture mechanics*, (Edward Arnold, London ISBN: 0-7131-3515-8, 1984) 88–90.
12) J. M. Krafft, A. M. Sullivan and R. W. Boyle: Proc. Of the Crack Propagation Symposium Cranfield, (the College of Aeronautics, England, 1, 1962) 8–28.